Shakeup in soft-x-ray emission. II. Plasmon satellites and x-ray photoemission spectroscopy

Peteris Livins and S. E. Schnatterly
Department of Physics, University of Virginia, Charlottesville, Virginia 22901
(Received 17 July 1987)

We report the first observation of a plasmon satellite in the K emission spectrum of diamond. The previously identified plasmon satellites of Al and graphite are also presented, and data is compared with an oscillator model applicable to soft-x-ray emission and photoemission. The graphite satellite is shown to exhibit an anomalous location with respect to the parent emission. We report for the Al $L_{\rm I}$-$L_{\rm II,III}$ core-core transitions a spin-orbit splitting of 0.42 ± 0.02 eV with a Lorentzian width of 0.67 ± 0.02 eV. The oscillator model applied to x-ray photoemission predicts a shift of the plasmon satellite with respect to the zero loss line as the final-electron kinetic energy is varied.

I. INTRODUCTION

The contribution of plasma oscillations in several experiments that probe the electronic structure of solids have been increasingly investigated during the past two decades. These experiments include x-ray photoemission spectroscopy (XPS),[1] soft x-ray emission (SXE),[2] Auger spectroscopy, appearance potential spectroscopy, and others. The effect is to produce a loss or gain, corresponding to the plasma energy, in the resulting spectra. The strength of the effect can be very strong, as demonstrated in XPS, or very small and difficult to observe, as in SXE. These plasmon satellites may be viewed as a collective shakeup event accompanying the primary electronic transition.

The previous paper,[3] which we refer to as I, introduced a discussion of shakeup in soft x-ray emission, but with regard to single-particle-like excitations. In soft x-ray emission, the plasmon satellites are observed to be 1–3 % of the main valence-band emission. Being this weak, and lying on a relatively large background, identification of these satellites is not as straightforward as in XPS, for instance. The choice of background subtraction significantly affects the line shape and overall strength. Therefore, experimentally, the plasmon satellites of SXE have rarely been carefully analyzed other than noting the approximate spectral location, with only approximate relative strengths. Being collective excitations, the plasmon satellites are a consequence of the electron-electron interaction. Several perturbative calculations[4–6] for the total emission of an interacting electron gas have been carried through, and a number of theoretical models[7–10] have been developed for the plasmon satellites of x-ray photoemission. Although several calculations[11–13] have been published specifically for the plasmon satellites of SXE, a simple model for fitting data in SXE has not appeared. We present such a model here.

For several years now, a number of investigators[14,15] have utilized the exact solution of the driven quantum oscillator in describing the plasmon satellites in x-ray photoemission. Recently Sokcevic and Sunjic,[9] through use of such a solution, obtain an XPS satellite line shape that includes the effects of both plasmon dispersion and damping. Unlike a first-principles perturbation approach, this technique requires some kind of phenomenological description of the density response to the sudden creation of a core hole and fast electron.

Little attention has been paid to the plasmon satellites of soft x-ray emission from this point of view. The aim here will be to discuss such a model applicable to SXE, and to comment on some qualitative points with regard to XPS. Specifically, we shall present recent data for aluminum, graphite, and diamond, and compare with the model. For XPS, we point out some effects of varying incident photon energy on the satellite line shape, with emphasis on the mutual screening between the photoelectron and the core hole.

II. OSCILLATOR MODEL

We assume the plasmons are independent elementary excitations, and although not necessary in our treatment here, for simplicity we assume isotropy in the plasmon wave-vector dependence. To obtain the satellite line shape then, we convolve the main emission band with a plasmon lineshape of a particular wave vector, and sum up the results for all wave vectors with the appropriate relative weights. The total transition rate $T(\nu)$ for emission is given by Eq. (1) in I. We construct the satellite transition rate $L(\nu)$ at energy ν with

$$L(\nu)=\int_0^{k_c}\int w(k,\nu')f(\nu')g_k(\nu'-\nu)\frac{\nu}{\nu'}d\nu'\,dk\ . \quad (1)$$

The parent emission transition rate is $f(\nu)$, and $g_k(E)$ is a plasmon line shape, of unit strength, for the wave vector $\mathbf{k}$ and energy loss E (as obtained from electron energy-loss spectra for instance). k_c is the plasmon cutoff vector and $w(k,\nu)$ is the wave vector weight function with primary emission at frequency ν; it is these weights that we will seek. The origin of the factor ν/ν' takes into account the frequency factor of Eq. (1) in I. Obviously, as pointed out in I, these frequency factors are important in comparing data with theory, and also when comparing with other data. Specifically, the plasmon satellite strengths are significantly affected by the manner in which data is plotted, and of course need to be consistent-

ly compared. Here, $T(\nu)$ and $L(\nu)$ will correspond to transitions per unit time per unit energy in arbitrary units, and we plot all emission data in such a manner.

The approach here, which borrows from concepts used in molecular spectra, is based on the standard electron gas formalism of Bohm and Pines.[16,17] There it was shown that the effects of electron interaction may be simplified by suitable unitary transformations that yield a Hamiltonian H of the form

$$H=\sum_i \frac{\mathbf{p}_i^2}{2m}+\sum_{k\le k_c}\tfrac{1}{2}(P_k^\dagger P_k+\omega_k^2 Q_k^\dagger Q_k)\ , \tag{2}$$

where $\mathbf{p}_i$ is the ith electron's momentum with m its mass, and P_k is the conjugate momentum of the coordinate Q_k. Here the Coulomb interaction between electrons has been removed, and its effects replaced with a set of harmonic oscillators with frequencies $\omega(k)$. These quanta are the plasmons, and the index k sums over the wave vectors for density fluctuations up to a cutoff k_c. Thus, the many-body wavefunction $|\Psi\rangle$ is a direct product of single particle states with these oscillator states.

If we consider the original Bohm and Pines (BP) Hamiltonian, but now include the possibility of a core hole which has a sufficiently long lifetime to be screened by the electron gas, then the following model Hamiltonian can be used:

$$H=\sum_i \frac{\mathbf{p}_i^2}{2m}+\tfrac{1}{2}\sum_k M_k^2(\rho_k^\dagger\rho_k-N)+\sum_{k\le k_c}\left[\frac{P_k^\dagger P_k}{2}-M_k P_k^\dagger\rho_k\right]+\sum_k M_k(F_k+G_k)\rho_k c^\dagger c-\sum_{k\le k_c}(F_k+G_k)P_k^\dagger c^\dagger c\ . \tag{3}$$

$M_k F_k$ and $M_k G_k$ represent the Fourier components of the interaction between a valence electron with the screening electrons and the ionic core, respectively, and where $M_k=(4\pi e^2/\Omega K^2)^{1/2}$ has been factored out for convenience. N is the total electron number, Ω the volume, e the electron charge and ρ_k is the kth Fourier component of the electron density. $c^\dagger$ and c are creation and annihilation operators for a core hole. The last term has been added to transform away the Coulomb interaction between the core hole and the electron gas when using the BP transformation $U=\exp(iS)$ with

$$S=\sum_{k\le k_c} M_k Q_k\rho_k\ , \tag{4}$$

and the subsidiary condition

$$P_k|\Psi\rangle=0\ . \tag{5}$$

The model Hamiltonian is then similar to that of Brouers,[12] except that a screening of the core hole has been included explicitly from the start. After transforming we obtain (besides the short-range, RPA and electron-plasmon interaction terms)

$$H=\sum_i \frac{\mathbf{p}_i^2}{2m}+\sum_{k\le k_c}\tfrac{1}{2}(P_k^\dagger P_k+\omega_p^2 Q_k^\dagger Q_k)-\sum_{k\le k_c}(F_k+G_k)P_k^\dagger c^\dagger c\ , \tag{6}$$

where $\omega_p^2=4\pi e^2 n/m$ and n is the valence electron density. The kth oscillator is perturbed by an effective field F_k+G_k. In the solution to this well-known problem, the zero for the oscillator coordinate P_k is translated by F_k+G_k, and an overall shift in the energy of $-\frac{1}{2}\sum_{k\le k_c}(F_k+G_k)^2$ arises due to the greater binding of the screening electrons. A further transformation[16] finally introduces the dispersion and renormalizes the electron mass.

We will be assuming that the potential felt by a valence electron near an ion undergoing an emission or absorption process may be determined by suitably modeling the dynamic variation of charge density as a result of the electronic transition. That description will provide a dynamic effective field perturbing the oscillators, and since an exact time-dependent solution to this problem is known, it may be utilized in calculating the relative probabilities of plasmon shakeup. Whether we discuss emission or absorption, the effective field changes from some initial value to a final value. Since the effective field translates the origin of the coordinate P_k, two complete sets of oscillator states are considered. The initial state is the ground state for the initial value of the effective field, and we are interested in obtaining the probability amplitude for the kth oscillator to be in the nth excited state in the set of states corresponding to the final value of the effective field. The zero of the effective field is chosen to correspond to the final-state electron density.

If we denote the difference between the initial and final values of F_k+G_k by Δ_k, then the initial oscillator state $|\phi_k\rangle=\sum_n \alpha_k^n|n\rangle$ is specified through expansion coefficients α_k^n, which are the overlap integrals

$$\alpha_k^n=\left[\frac{1}{2^n n!\pi\hbar\omega_k}\right]^{1/2}\int_{-\infty}^{\infty}\exp\left[\frac{-(P_k-\Delta_k)^2}{2\hbar\omega_k}\right]\times\exp\left[\frac{-P_k^2}{2\hbar\omega_k}\right]H_n\left[\frac{P_k}{(\hbar\omega_k)^{1/2}}\right]dP_k \tag{7}$$

between the translated ground state and the untranslated oscillator state $|n\rangle$. H_n is a Hermite polynomial. The integral gives

$$\alpha_k^n=\left[\frac{\Delta_k}{(2\hbar\omega_k)^{1/2}}\right]^n\frac{\exp[-\Delta_k^2/(4\hbar\omega_k)]}{(n!)^{1/2}}\ . \tag{8}$$

The temporal development at time t is determined by the operator[18]

$$U(t)=\exp[-i\omega_k t(a_k^\dagger a_k+\tfrac{1}{2})+C_k(t)a_k^\dagger-C_k^*(t)a_k+A_k(t)]\ , \tag{9}$$

where

$$A_k(t)=-\frac{\omega_k}{2\hbar}\int_0^t f_k(t')\exp(-i\omega_k t')\times\int_0^{t'} f_k^*(t'')\exp(i\omega_k t'')dt''dt' , \tag{10}$$

$$C(t)=i\left[\frac{\omega_k}{2\hbar}\right]^{1/2}\int_0^t f_k(t')\exp(i\omega_k t')dt' , \tag{11}$$

$$f_k(t)=F_k(t)+G_k(t) . \tag{12}$$

The $a^\dagger$ and a are the usual boson creation and annihilation operators defined in this case by

$$a_k=\left[\frac{1}{2h\omega_k}\right]^{1/2}(P_k-i\omega_k Q_k) , \tag{13}$$

$$a_k^\dagger=\left[\frac{1}{2h\omega_k}\right]^{1/2}(P_k^\dagger+i\omega_k Q_k^\dagger) , \tag{14}$$

having the property

$$a_k\mid n\rangle=\sqrt{n}\mid n-1\rangle , \tag{15}$$

$$a_k^\dagger\mid n\rangle=\sqrt{n+1}\mid n+1\rangle . \tag{16}$$

The amplitude γ_k^n for the kth oscillator to be in the nth excited state is obtained through evaluating

$$\gamma_k^n(t)=\langle n\mid U(t)\mid\phi_k(t=0)\rangle , \tag{17}$$

with Eq. (9). Repeated application of the above property for a and $a^\dagger$ (Eqs. 15 and 16) with some algebra give

$$\gamma_k^n(t)=\exp\left[-i\omega t(n+\tfrac{1}{2})+A_k(t)-\frac{\Delta_k^2}{4\hbar\omega_k}-\frac{C_k^*(t)\Delta_k}{(2\hbar\omega_k)^{1/2}}\right]\times\left[\frac{\Delta_k}{(2\hbar\omega_k)^{1/2}}+C_k(t)\right]^n/\sqrt{n!} . \tag{18}$$

The amplitude at time t, that n plasmons will be excited corresponding to the kth oscillator while other oscillators remain in their ground state is determined by considering the product

$$\gamma_k^n\prod_{\mathbf{q}\neq\mathbf{k}}^{k_c}\gamma_q^0=\frac{\gamma_k^n}{\gamma_k^0}\prod_{\mathbf{q}}^{k_c}\gamma_q^0 . \tag{19}$$

Here, and in what follows, γ_k^n is $\gamma_k^n(\infty)$. If we take the logarithm and exponentiate, the squared modulus of the above becomes

$$\left|\frac{\gamma_k^n}{\gamma_k^0}\prod_{\mathbf{q}}^{k_c}\gamma_q^0\right|^2=\left|\frac{\gamma_k^n}{\gamma_k^0}\right|^2\exp\left[2\,\mathrm{Re}\int_0^{k_c}\ln(\gamma_k^0)\frac{\Omega k^2}{2\pi^2}dk\right] . \tag{20}$$

The exponential in Eq. (20) is the probability for no plasmon shakeup. It will be dropped since we need only the relative probabilities. In the simple case when satellite coupling is independent of the final valence hole [$w(k,\nu)=w(k)$], we may sum over all wave vectors to obtain the total relative integrated first satellite strength $P(1)$,

$$P(1)=\int_0^{k_c}\left|\frac{\gamma_k^1}{\gamma_k^0}\right|^2\frac{\Omega k^2}{2\pi}dk . \tag{21}$$

It is now evident that the weight function $w(k)$ is given by

$$w(k)=\left|\frac{\gamma_k^1}{\gamma_k^0}\right|^2\frac{\Omega k^2}{2\pi}=\mid\eta_k^1\mid^2\frac{\Omega k^2}{2\pi} , \tag{22}$$

where we have defined

$$\eta_k^n=\left[\frac{\Delta_k}{(2\hbar\omega_k)^{1/2}}+C_k\right]^n/\sqrt{n!} . \tag{23}$$

Furthermore, due to the factorial of Eq. (23), we may write the total integrated relative probability for exciting n plasmons in all possible ways as

$$P(n)=\frac{1}{n!}\int_0^{k_c}\left[\frac{\Omega}{2\pi^2}\right]^n\times\mid\eta_{k_1}^1\cdots\eta_{k_n}^1\mid^2 k_1^2\cdots k_n^2\,dk_1\cdots dk_n=\frac{1}{n!}\left[\int_0^{k_c}\mid\eta_k^1\mid^2\frac{\Omega k^2}{2\pi^2}dk\right]^n . \tag{24}$$

The satellite strengths follow a Poisson distribution.

In photoemission, it has been customary to distinguish between two types of satellite contributions: coupling to the core hole and coupling to the photoelectron. We need to properly consider the interference between such contributions. The effective field does just that; it corresponds to the superposition of particle density, but also includes their electrical charge. Coupling to the hole and the electron are of opposite phase (charge); hence the interference is destructive. Of course, the physical ingredient needed is a model for the effective field.

III. SXE PLASMON SATELLITES

In the case of emission, a positively charged core hole is surrounded by a negative screening cloud which essentially cancels the interaction with a "passing" valence electron. Some electrons eventually make a radiative transition, eliminating the core hole, but immediately leaving a valence hole in its place. The response of the electronic system is not instantaneous, but of the order of the plasma oscillation period. Furthermore, the valence hole may move away from the original site, contributing to the dynamic effective field. Thus initially the screening density is distributed for essentially a point charge, and must then try to adjust itself to the extended valence hole. As the valence hole moves away the electron density must further do its best to keep it screened.

We shall model this state of affairs by first assuming Fermi-Thomas screening of a positive point charge. At $t=0$ the point charge becomes a spherical shell of positive charge with a finite radius r_0. The radius then increases at a rate corresponding to some velocity v up to the Fermi velocity. After an appropriate screening time, the expanding shell of charge is considered to be statical-

ly screened. The static screening should be good for velocities less than the Fermi velocity, but becomes more dubious when the Fermi velocity is approached.

For emission, the corresponding effective field we use is

$$f_k(t)=-M_k\left[\left[\frac{\sin[k(r_0+vt)]}{k(r_0+vt)}-\frac{k_0^2}{k^2+k_0^2}\right]\times\exp(-\omega_k t/2\pi)+\left[\frac{k^2\sin[k(r_0+vt)]}{(k^2+k_0^2)k(r_0+vt)}\right]\times[1-\exp(-\omega_k t/2\pi)]\right]. \quad (25)$$

Here, we turn off the initial effective field exponentially with a time constant equal to a plasma period. Simultaneously the effective field due to a statically (Fermi-Thomas) screened expanding shell of positive charge is turned on exponentially. The velocity of the expanding radius is determined by the valence hole energy within the bandwidth of the parent emission. We use $v=v_F(\varepsilon/\varepsilon_F)^{1/2}$, where ε is the valence energy measured from the valence-band minimum, and ε_F with v_F are the corresponding Fermi energy and Fermi velocity. The radius r_0 corresponds to the initial finite spacial extent of the valence hole, and k_0 is the Fermi-Thomas wave vector. A suitable choice for r_0 is the average radius of a self-consistent atomic wave function. In those cases when the valence state is considered a linear combination of an s and p state, we vary the value of r_0 from the s value to the p value in a linear manner [Eq. (28) for instance] as the valence hole energy is varied from the band minimum to the Fermi energy. Thus v and r_0 introduce the ν dependence in the weight function $w(k,\nu)$. The integral of Eq. (11) is evaluated numerically. For $v=0$ the integral does not strictly converge for our choice of $f_k(t)$. We use a cutoff of $40\pi/\omega_k$, since a more properly modeled effective field would go to zero with increasing time.

In applying this model, we will need information about the **k** dependence of the plasmon energy and width, not to mention the cutoff vector. We will describe these quantities with the following **k** dependence:

$$\omega_k=\omega_0+\mu k^2 , \quad (26)$$

$$\Gamma_k=\Gamma_0+\xi k^2 . \quad (27)$$

Γ_k is the full width at half maximum as a function of k, Γ_0 and ω_0 are values, at $\mathbf{k}=0$, of the plasmon width and energy respectively.

As discussed in I, the plasmon satellites of soft x-ray emission rest upon a background which is due to single-particle-like shakeup and to a lifetime-broadened parent band emission. In previous measurements of these satellites a reasonable background was arbitrarily drawn under the satellite and subtracted to obtain the satellite line shape and strength.[20,21] In I we discuss a method for determining this background with at least some physical principles in mind, and have applied it to the satellites observed in aluminum, graphite and diamond. The resultant data with the background subtracted is pictured in Figs. 1(b) and 2, along with calculated line shapes.

For aluminum, the L_I-$L_{II,III}$ core-core transition[19] interferes with the satellite emission. We have fit two spin-orbit split Lorentzians on a linear background to this peak [Fig. 1(a)]. The Lorentzian higher in energy was fixed to have exactly twice the strength as the other. We are then able to resolve the spin-orbit splitting, and obtain 0.42±0.02 eV, with a Lorentzian width of 0.67±0.02 eV. The location of the L_I-L_{III} peak was observed to be at 45.22±0.05 eV.

After subtracting the core-core transition, the integrated satellite strength is 2.2±0.2% of the main emission integrated from 62 to 73 eV. The first observation of this satellite was due to Rooke.[20] He quotes peak-to-peak ratios for Al, Mg, and Na as 1.0%, 1.2%, and 2.0%, respectively, with a large uncertainty. Besides Rooke, a published plasmon satellite for aluminum has also been provided by Neddermeyer and Wiech.[21] Although they do not quote its relative strength, our analysis of their published data gives a corresponding integrated strength of 2.0%.

Parameters for modeling the aluminum plasmon satellite are determined by considering electron energy-loss data. Our inelastic electron scattering data for aluminum have been fit according to Eqs. (26) and (27), and we obtain $\omega_0=15.05$ eV, $\Gamma_0=0.6$ eV, $\mu=2.6$ eV Å^2, and $\xi=1.5$ eV Å^2. Self-consistent atomic wave functions[22] give the mean radii for $3s$ and $3p$ Al states as 1.3 and 1.7 Å, respectively. We model r_0 for aluminum as

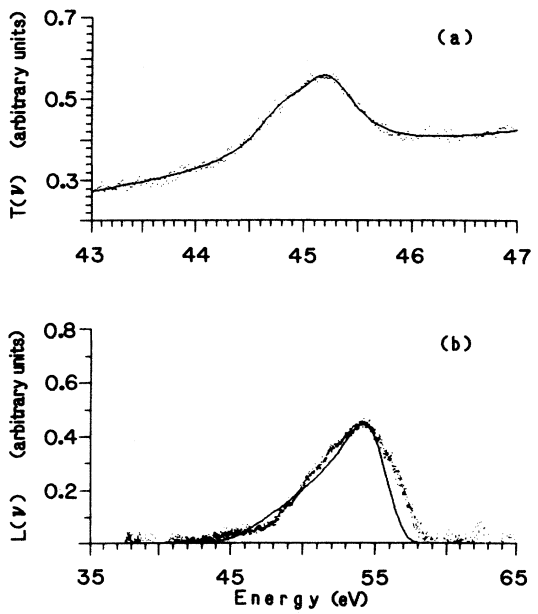

FIG. 1. (a) Soft x-ray L emission data for aluminium in the region of the L_I-$L_{II,III}$ core transitions (dots). The solid line is the spin-orbit split Lorentzian fit. (b) The aluminum plasmon satellite (dots) with low-energy tail and core-core transition subtracted. The solid line is the modeled aluminum plasmon satellite.

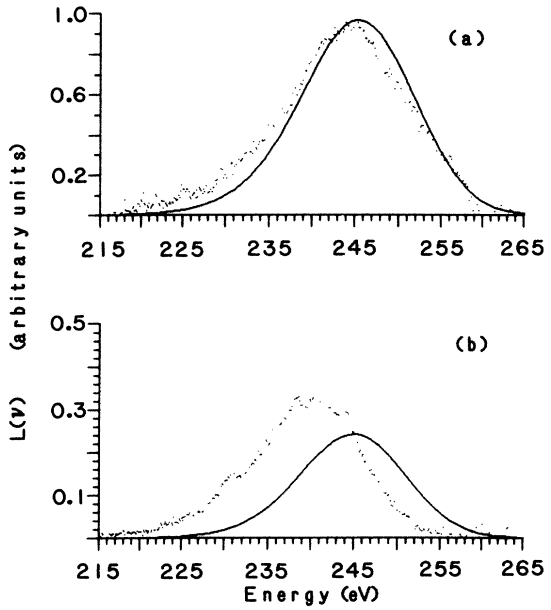

FIG. 2. (a) The diamond plasmon satellite (dots) with low-energy tail subtracted. The solid line is the modeled diamond plasmon satellite. (b) The graphite plasmon satellite (dots) with the low energy tail subtracted. The solid line is the modeled graphite plasmon satellite.

spectively. We model r_0 for aluminum as

$$r_0 = 1.3 + 0.4\varepsilon/\varepsilon_F \ , \tag{28}$$

with similar linear relations for other materials. Following Gibbons *et al.*,[23] we use a cutoff wave vector of 1.1 Å^{-1}. Equations (25) and Eq. (11) give the weight function according to Eq. (22). Fermi-Thomas screening determines Δ_k, and the final line shape is determined with Eq. (1), where we use normalized Gaussians centered at ω_k for $g_k(\nu)$. Our calculated integrated relative strength of 1.9% is in close agreement with the observed value, and the line shape depicts the data satisfactorily. The success of this simple model on the test case of aluminum provides encouragement for its use on other materials.

Several earlier measurements[24,25] have identified a plasmon satellite in the emission of graphite. We have observed such a feature in both graphite and diamond. These satellites, with the backgrounds of I subtracted appear in Fig. 2. Here we compare these features with the present plasmon satellite model, although some dispersion information is lacking. Graphite is anisotropic, and its dispersion parameters have not yet been measured along the c axis; furthermore, dispersion parameters for diamond are nonexistent. We have fit Buchner's[26] electron energy-loss data for graphite, according to Eqs. (26) and (27), for the plasmon dispersion in both directions perpendicular to the c axis. Averaging the two directions for use in Eqs. (26) and (27), we find $\omega_0 = 27.45$ eV, $\mu = 4.2$ eV Å^2, $\Gamma_0 = 10$ eV, and ξ is essentially zero. For diamond we will simply note that for large-band-gap insulators the dispersion is typically small or zero.[27] Not having any more information, we will use the $\mathbf{k}=0$ values of $\omega_0 = 33.3$ eV and $\Gamma_0 = 13$ eV measured by Egerton and Whelan[28] and take both μ and ξ equal to zero. Since no measured determination of a cutoff vector is currently available, in both cases we use the Ferrell value of $k_c = 0.471 k_F (r_s^{1/2})$ where $r_s = (1/a_0)(3/4\pi n)^{1/3}$, with a_0 the Bohr radius and k_F the Fermi vector. For diamond and graphite, k_c is then 1.49 and 1.38 Å^{-1}, respectively. The $2s$ and $2p$ mean radii for carbon self-consistent atomic functions are 0.81 and 0.89 Å, respectively.

The integrated relative strength of the satellite in diamond was measured to be 1.6±0.2% of the main emission integrated from 258 to 264 eV. The calculated plasmon satellite for diamond appears to fit well with the observed satellite, and room remains for an even better fit if a slight dispersion were included. The calculated integrated relative strength is 1.75%. Thus little doubt remains that the satellite in diamond is indeed due to plasmon shakeup.

The result of our model calculation for graphite is not as satisfying. The observed integrated relative strength is 1.2±0.15% of the main emission integrated from 263 to 285 eV. Our calculated integrated relative strength is reasonably close, with 0.9%. Also, the overall shape and width appear to match the observed satellite. However, the location of the observed satellite is lower in energy by approximately 4 eV from the modeled position. Although the dispersion along the c-axis was not properly taken into account, it appears that doing so would only serve to move the calculated satellite higher in energy, since Venghaus[29] has measured the $\mathbf{k}=0$ electron energy-loss spectra for graphite along the c-axis and finds the plasma loss at 20 eV. Besides the discrepancy in location, the overall strength, shape, and width of the feature do agree reasonably well with our plasmon satellite model. Unlike the candidate for a plasmon satellite for silicon discussed in I, the anomalous position in graphite is in a direction permissible due possibly to some unusual dispersion or large cutoff vector. We therefore assign a plasmon satellite to this feature in graphite, in agreement with the earlier identifications, but we point out the anomalous position for which we have no explanation.

In I, we identified a low-energy feature in silicon as due to structure in the single-particle-like shakeup, and refuted the plasmon satellite identification it had been previously assigned to. In doing so we modeled a plasmon satellite in silicon with the presently discussed method. The location of the observed feature was far too high in energy and completely inconsistent with the well-documented silicon plasma loss and dispersion. The modeled silicon plasmon satellite appears in Fig. 8 of I, with the dispersion parameters $\omega_0 = 16.97$ eV, $\Gamma_0 = 2.0$ eV, $\mu = 2.6$ eV Å^2, $\xi = 3.35$ eV Å^2, and the Ferrel cutoff vector. The $3s$ and $3p$ values for r_0 used were 1.12 and 1.42 Å, respectively. We do, however, point out that a weak silicon plasmon satellite might be present, but that it should be difficult to observe next to the single-particle-like shakeup structure.

IV. XPS PLASMON SATELLITES

Although we have been mainly concerned with plasmon shakeup in SXE spectra, we may modify the

present description in order to make some comments about XPS plasmon satellites. To do so, we need a reasonable model for the dynamic effective field for the photoemission process. Such a procedure will yield interesting physics when the photon energy is variable. This will characterize the plasmon shakeup as the time scales vary from the adiabatic to sudden limit.

For photoemission, an electron at some core site is excited to a continuum state that is initially localized about the core hole, then it proceeds to move away with a velocity corresponding to its kinetic energy. The response of the surrounding electrons will be to produce density fluctuations that attempt to screen the newly created charges. The screening is maximally achieved in the case of the stationary core hole, but the degree of screening for the moving electron decreases with velocity.

While the photoelectron is still near the site, the remaining core hole and escaping electron screen one another, at which point the effective field seen by the plasmons is relatively small. If the electron velocity is great enough that it leaves the proximity of the core hole before a screening time has elapsed, it will leave behind an unscreened positive charge, thereby creating a strong effective field. When the stationary core hole is later completely screened by the surrounding electron gas, any screening provided to the photoelectron is lost, and the moving unscreened photoelectron may produce plasmons until it escapes through the surface, where it might also excite a surface plasmon.

For the effective field in photoemission we use the function

$$f(t)=-M_k\left[1-\frac{\sin(kvt)}{kvt}-\frac{k^2}{k^2+k_0^2}\right]\exp(-\omega_k t/2\pi)\ . \tag{29}$$

This function, excluding the exponential, corresponds to a stationary positive point charge (the core hole) and a concentric negative shell of charge expanding radially outward with velocity v (the photoelectron). The effective field zero is referred to the final Fermi-Thomas screened state. The screening of the core hole is achieved by the exponential, with the time constant $\omega_k/(2\pi)$. The exponential also screens the photoelectron, turning off the coupling to the photoelectron after a screening time. We then neglect to model the inelastic scattering of the photoelectron after a screening time. We instead only include the photoelectron during times in which it can interfere with the core hole. After this point, if the photoelectron has not already escaped to the surface, plasmons can be excited by the electron acting independently. In a more complete treatment, one would include the later contribution by averaging over core sites, and using a mean free path to weight contributions at different depths.[9]

As mentioned earlier, the contributions to the satellite strengths may be viewed as individual coupling to the core hole, the photoelectron, and their mutual interference. Earlier workers[7,30] have termed plasmon coupling to the photoelectron as the extrinsic contribution, while coupling to the core hole together with the interference was termed the intrinsic contribution. Our model function not only represents the inclusion of the intrinsic contribution, it includes the extrinsic contribution for times during which the two are able to interfere. We have instead modeled the coupling to the core hole and photoelectron as a one-step process during times that it is most important to do so. For kinetic energies of 50 eV or more, electron escape depths[31] are comparable to the distance that an electron travels in a screening time, thus neglecting the later inelastic scattering of the photoelectron should be a reasonable approximation.

Using Eq. (29) we have calculated the satellite strengths for Al, Mg, and Na, as a function of photoelectron kinetic energy. The dispersion parameters used for Mg are $\omega_0=10.2$ eV, $\mu=2.6$ eV Å^2, $\Gamma_0=0.7$ eV, $\xi=1.1$ eV Å^2, and for Na, $\omega_0=5.6$ eV, $\mu=1.9$ eV Å^2, $\Gamma_0=0.4$ eV, and $\xi=2.0$ eV Å^2. In both cases we use the Ferrell cutoff vector. The results, along with some published[32,33] experimental data appear in Fig. 3. The curves first increase with low kinetic energy in the adiabatic regime, to an asymptotically approached constant as the sudden limit is attained. The depiction of the data is quite good for such a crude model. The calculated strengths are slightly weaker, quite possibly indicating the missing late inelastic scattering contribution.

Several years ago Penn[34] introduced a particular three-step model that ignored the interference of the intrinsic and extrinsic contributions. For high photoelectron energies, it would be expected that the present model would provide strengths that are similar to the intrinsic contributions of Penn, for in this limit, the present model simulates the sudden appearance of a positive point charge with little mutual screening between it and the photoelectron. This seems to be the case, since Penn reports intrinsic strengths for Al, Mg, and Na as 26%, 36%, and 41%, respectively, while our calculated corresponding strengths are 26%, 38%, and 56%. Penn's good agreement with experiment would suggest that the interference is negligible for hard x rays. Modeling the intrinsic contribution with the sudden appearance of a

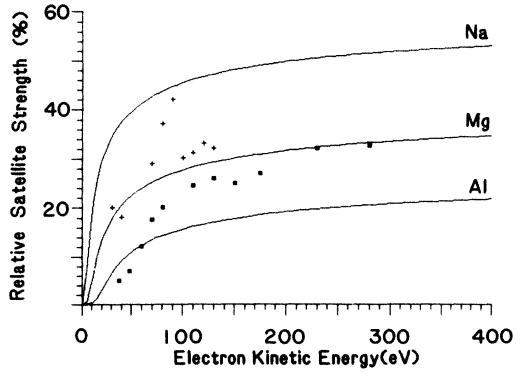

FIG. 3. The modeled XPS plasmon satellite strengths for Al, Mg, and Na, as a function of the electron kinetic energy. The solid points are data for Al from Johansson and Lindau (Ref. 32). The crosses are data for Mg from Norman and Woodruff (Re. 33).

point charge alone implicity assumes that the interference does not exist, since the sudden appearance of a point charge with its full unscreened potential alone implies no photoelectron is in the vicinity to provide such interference, a situation which is realistic for hard x rays. For soft x rays, the present analysis indicates that the interference is essential.

We plot for aluminum in Fig. 4, the wave-vector weight function for two incident photon energies in exciting photoelectrons from the $2p$ core, which is bound by ≈ 73 eV. An escaping electron that has involved a plasma excitation, has a kinetic energy of ≈ 1412 eV due to a 1500-eV photon. For such a velocity, the wave-vector weight function is negligible at small k, then rises sharply at approximately $k \approx \omega_k / v$, which is 2π multiplied by the inverse distance that the electron travels in a screening time. A similar behavior is demonstrated for the 150-eV incident photon. In this case the electron kinetic energy is ≈ 62 eV, thus the photoelectron does not travel as far in a screening time and the corresponding rise in the weight function occurs at greater k. In our model the distance the electron travels in a screening time is the extent of the newly created charge distribution. This maximum extent corresponds to the minimum density fluctuation wave vector needed in the screening, and thus not all plasmons with different wave vectors are excited. In the case of fast electrons, plasmons of almost all wave vectors are weighted comparably. This is in contrast to SXE, where plasmons nearer k_c are weighted more heavily.

An interesting measurable consequence with this XPS model is predicted due to the plasmon energy dispersion with wave vector. The first moment of the satellite line shape, measured from the zero loss line, should "disperse" with incident photon energy. We express this moment $m(E)$, for an escaping electron of kinetic energy E and wave vector weight function $w(k,E)$ with,

$$m(E)=\int_0^{k_c} \hbar\omega_k w(k,E)dk \Big/ \int_0^{k_c} w(k,E)dk \ . \quad (30)$$

A plot of this function appears in Fig. 4 for the case of aluminum with the above mentioned dispersion parameters. The centroid of the weight function increases in going from high kinetic energies toward lower kinetic energies. A casual inspection of the published data of Flodstrom *et al.*[35] exhibits such a dispersion. Below the plasma energy the trend reverses, essentially because here the effective field for the greater oscillator energies changes significantly more adiabatically than for the lower energies. Hence, the excitation probabilities of the smaller-wave-vector plasmons are relatively enhanced compared to the greater-wave-vector plasmons.

Figure 5 displays the modeled Al XPS $2p$ core plasmon satellite line shapes for several incident photon energies before convolving with a zero loss line, and ranging over the adiabatic to sudden transition. The mentioned dispersion is evident, and would be most easily perceived with incident soft x rays. The line shape corresponding to the 1500-eV photon has some distinctive structure. The sharp peaking is a consequence of the equal weighting of almost all the wave vectors, together with a quadratic plasmon energy dispersion.

V. SUMMARY

We have discussed a model for the analysis of plasmon satellites in soft x-ray emission which we compare with recent measurements on Al, graphite, and diamond. The model confirms the plasmon satellite identification of the low-energy features, but also points out an anomalous shift in the graphite satellite.

We have also investigated several aspects of plasmon satellites in XPS with particular emphasis on the mutual screening between the core hole and photoelectron as the incident photon energy is varied. The analysis predicts a dispersion of the satellite strength away from the zero loss line as the photon energy is decreased through the

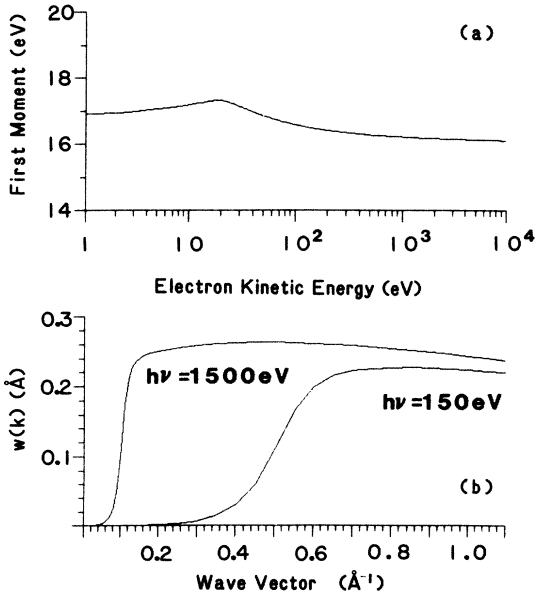

FIG. 4. (a) Modeled first moment of the XPS $2p$ core Al plasmon satellite line shape with respect to the zero loss line as a function of the electron kinetic energy. (b) The wave vector weight function for the XPS $2p$ core Al plasmon satellite for 1500- and 150-eV incident photons.

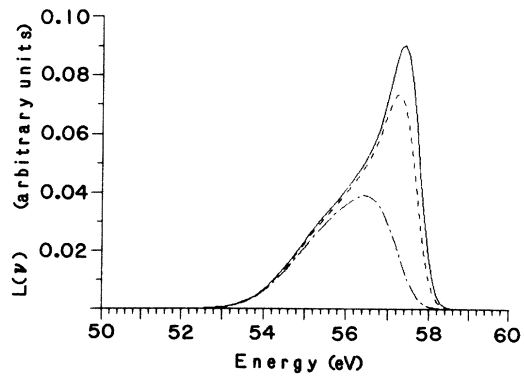

FIG. 5. The modeled XPS $2p$ core Al plasmon satellite line shapes for a 1500-eV photon(solid line), 500-eV photon(dashed line) and a 150-eV photon(dashed-dotted line).

soft x ray region. Our result suggests why the neglect of interference between the intrinsic and extrinsic contributions of Penn's theory is a good approximation.

ACKNOWLEDGMENTS

We would like to thank P. Bruhwiler, R. Carson, D. Husk, A. Mansour, J. Nithianandam, C. Tarrio, S. Velasquez, Dr. T. Aton and A. Cafolla, for helpful suggestions and discussions throughout the course of this work. We are also grateful to Dr. H. P. Kelly and M. Kutzner for access to the self-consistent atomic calculations. This research was supported in part by the National Science Foundation (Grant No. DMR 85-15684).

[1]L. Ley and M. Cardona, *Photoemission in Solids II* (Springer-Verlag, Berlin, 1979).
[2]D. J. Fabian, *Soft X-ray Band Structure* (Academic, New York, 1968).
[3]Peteris Livins and S. E. Schnatterly, preceding paper, Phys. Rev. B **37**, 6731 (1988).
[4]P. Longe and A. J. Glick, Phys. Rev. **177**, 526 (1969).
[5]B. Bergersen, F. Brouers, and P. Longe, J. Phys. F **1**, 945 (1971).
[6]S. M. Bose and A. J. Glick, Phys. Rev. B **10**, 2733 (1974).
[7]J. J. Chang and D. C. Langreth, Phys. Rev. B **8**, 4638 (1973).
[8]G. D. Mahan, Phys. Status Solidi **55**, 703 (1973).
[9]D. Sokcevic and M. Sunjic, Phys. Rev. B **30**, 6965 (1984).
[10]C. Noguera and J. Friedel, J. Phys. F **12**, 2973 (1982).
[11]R. A. Ferrel, *Plasmon Excitation in X-ray Emission,* University of Maryland Technical Report No. 485, 1965 (unpublished).
[12]F. Brouers, Phys. Status Solidi **22**, 213 (1967).
[13]Y. Ohmura, J. Phys. Soc. Jpn. **30**, 1300 (1971).
[14]M. Sunjic, Phys. Scr. **1**, 561 (1980).
[15]A. M. Bradshaw, W. Domcke, and L. S. Cederbaum, Phys. Rev. B **16**, 1480 (1977).
[16]D. Bohm and D. Pines, Phys. Rev. **92**, 609 (1953).
[17]D. Pines, *Elementary Excitations in Solids* (Benjamin-Cummings, Reading, Mass., 1963).
[18]W. H. Louisell, *Radiation and Noise in Quantum Mechanics* (McGraw-Hill, New York, 1964).
[19]V. A. Fomichev, Fiz. Tverd. Tela (Leningrad) **8**, 2892 (1966) [Sov. Phys.—Solid State **8**, 2312 (1966)].
[20]G. A. Rooke, Phys. Lett. **3**, 234 (1963).
[21]H. Neddermeyer and G. Wiech, Phys. Lett. **31A**, 17 (1970).
[22]C. Froese-Fischer, Computer Phys. Commun. **14**, 145 (1978).
[23]P. C. Gibbons, S. E. Schnatterly, J. J. Ritsko, and J. R. Fields, Phys. Rev. B **13**, 2451 (1976).
[24]O. Aita, I. Nagakura, and T. Sagawa, J. Phys. Soc. Jpn. **30**, 516 (1971).
[25]M. A. Blokhin, E. G. Orlova, and I. G. Sveitser, Fiz. Tverd. Tela (Leningrad) **14**, 2475 (1973); [Sov. Phys.—Solid State **14**, 2146 (1973)].
[26]U. Buchner, Phys. Status Solidi **81**, 227 (1977).
[27]I. Egri, J. Phys. C **18**, 1191 (1985).
[28]R. F. Egerton and M. J. Whelan, Philos. Mag. **30**, 739 (1974).
[29]H. Venghaus, Phys. Status Solidi **71**, 609 (1975).
[30]M. Sunjic and D. Sokcevic, Solid State Commun. **18**, 373 (1976).
[31]I. Lindau and W. E. Spicer, J. Electron Spectrosc. **3**, 409 (1974).
[32]L. I. Johansson and I. Lindau, Solid State Commun. **29**, 379 (1979).
[33]D. Norman and D. P. Woodruff, Surf. Sci. **79**, 76 (1979).
[34]D. R. Penn, Phys. Rev. Lett. **38**, 1429 (1977).
[35]S. A. Flodstrom, R. Z. Bachrach, R. S. Bauer, J. C. Mcmenamin, and S. B. M. Hagstrom, J. Vac. Sci. Technol. **14**, 303 (1977).